Supporting Information

The Power of the Ring: pH-Responsive Hydrophobic Epoxide Monomer for Superior Micelle Stability

*Jaeeun Song,[1] L. Palanikumar,[1] Yeongkyu Choi,[1] Inhye Kim,[4] Tae-young Heo,[5] Eungjin Ahn,[2] Soo-Hyung Choi,[5] Eunji Lee,[4] Yuji Shibasaki,[3] Ja-Hyoung Ryu,[1] and Byeong-Su Kim[1,2]**

[1]Department of Chemistry, Ulsan National Institute of Science and Technology (UNIST), Ulsan 44919, Korea

[2]Department of Energy Engineering, Ulsan National Institute of Science and Technology (UNIST), Ulsan 44919, Korea

[3]Department of Chemistry and Bioengineering, Faculty of Engineering, Iwate University, 4-3-5 Ueda, Morioka, Iwate 020-8551, Japan

[4]Graduate School of Analytical Science and Technology, Chungnam National University, Daejeon 34134, Korea

[5]Department of Chemical Engineering, Hongik University, Seoul 04066, Korea

E-mail: bskim19@unist.ac.kr

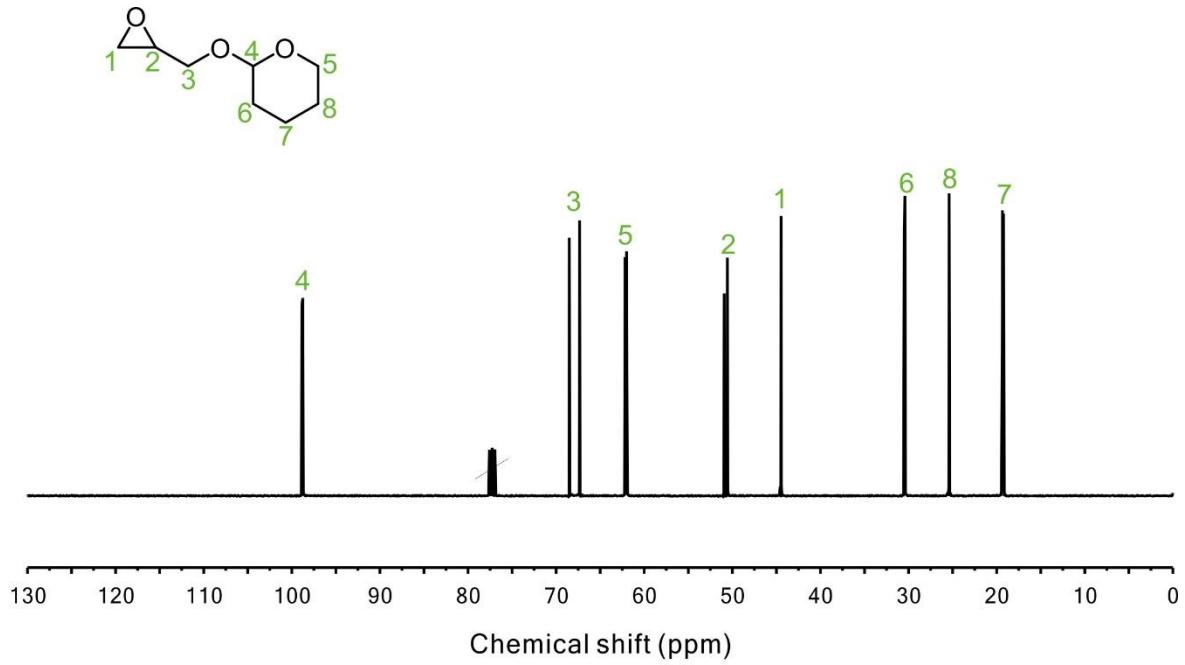

Fig. S1 ^{13}C NMR spectrum of TGE monomer (100 MHz, $CDCl_3$).

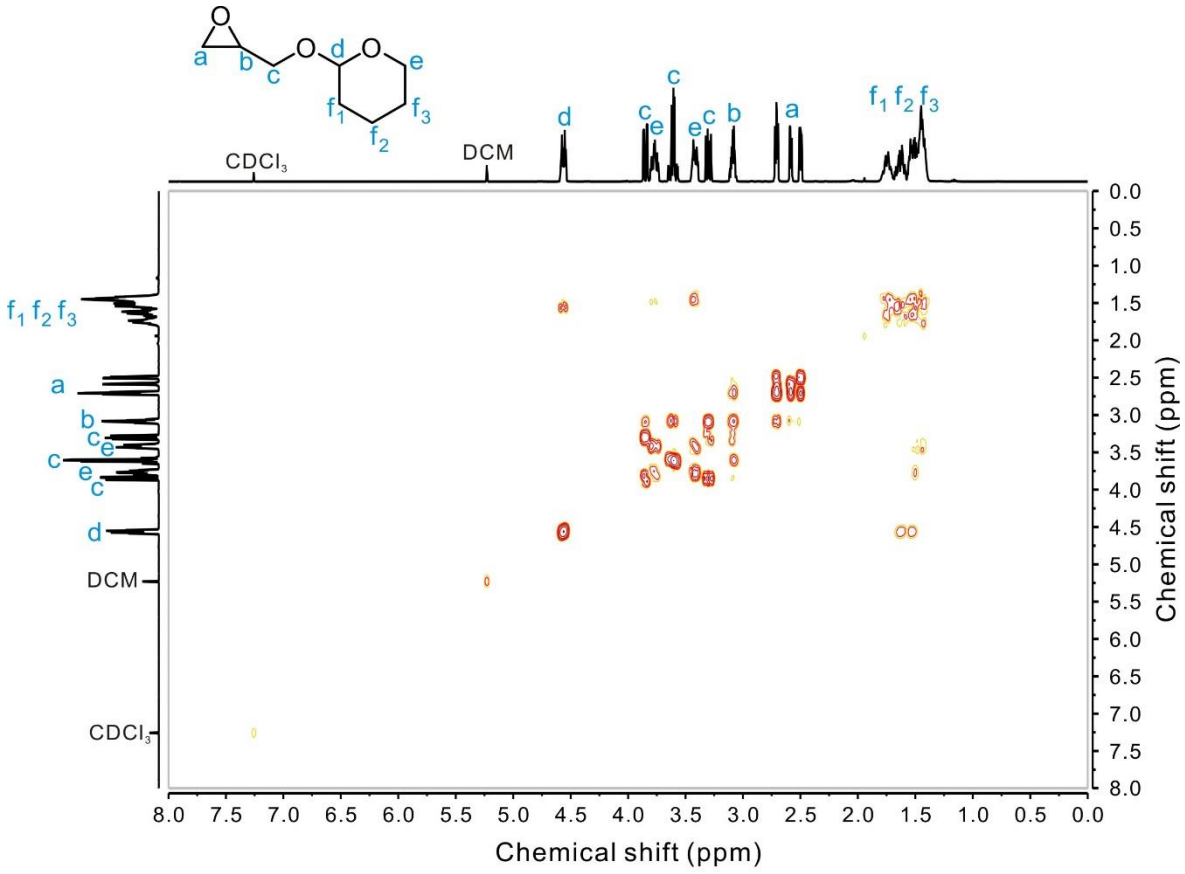

Fig. S2 ^{1}H-^{1}H COSY NMR spectrum of TGE in $CDCl_3$.

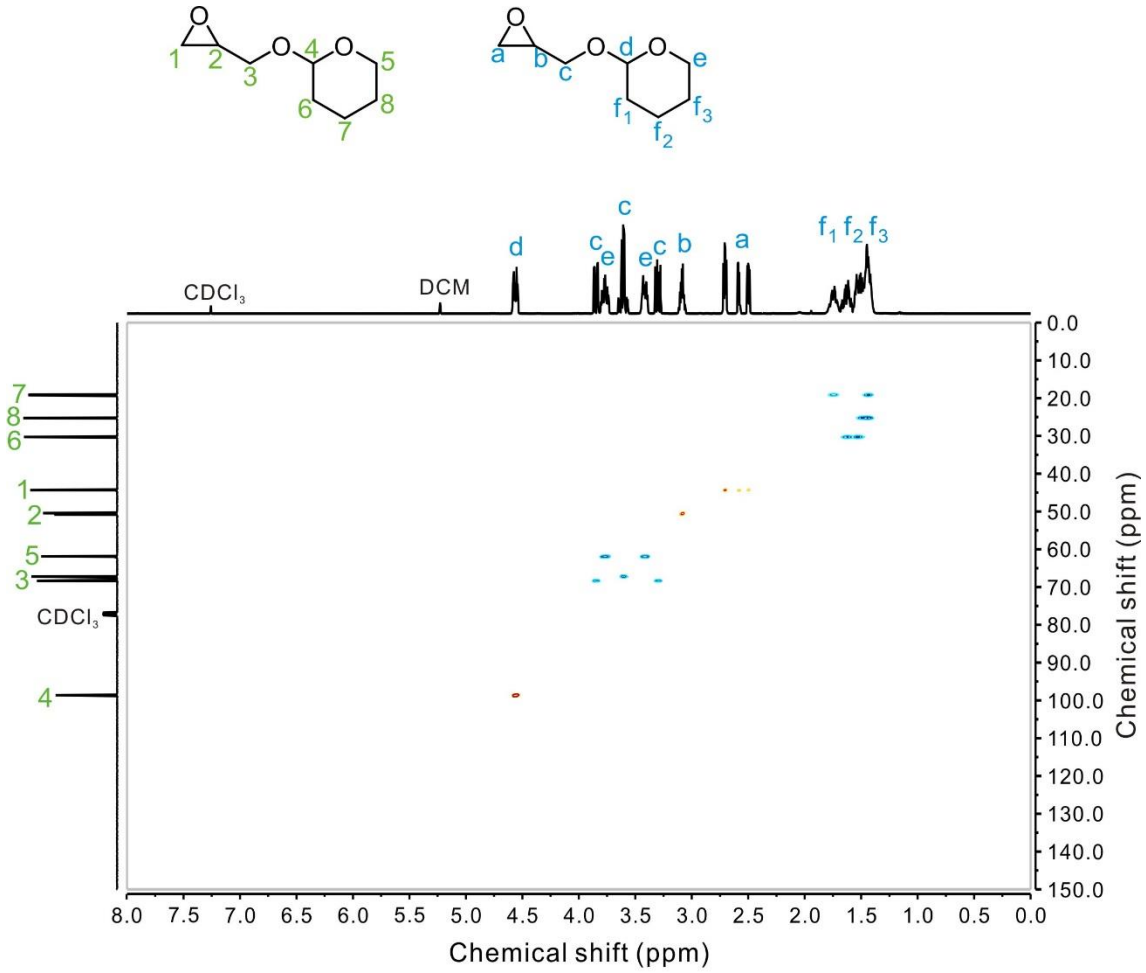

Fig. S3 HSQC NMR spectrum of TGE in $CDCl_3$.

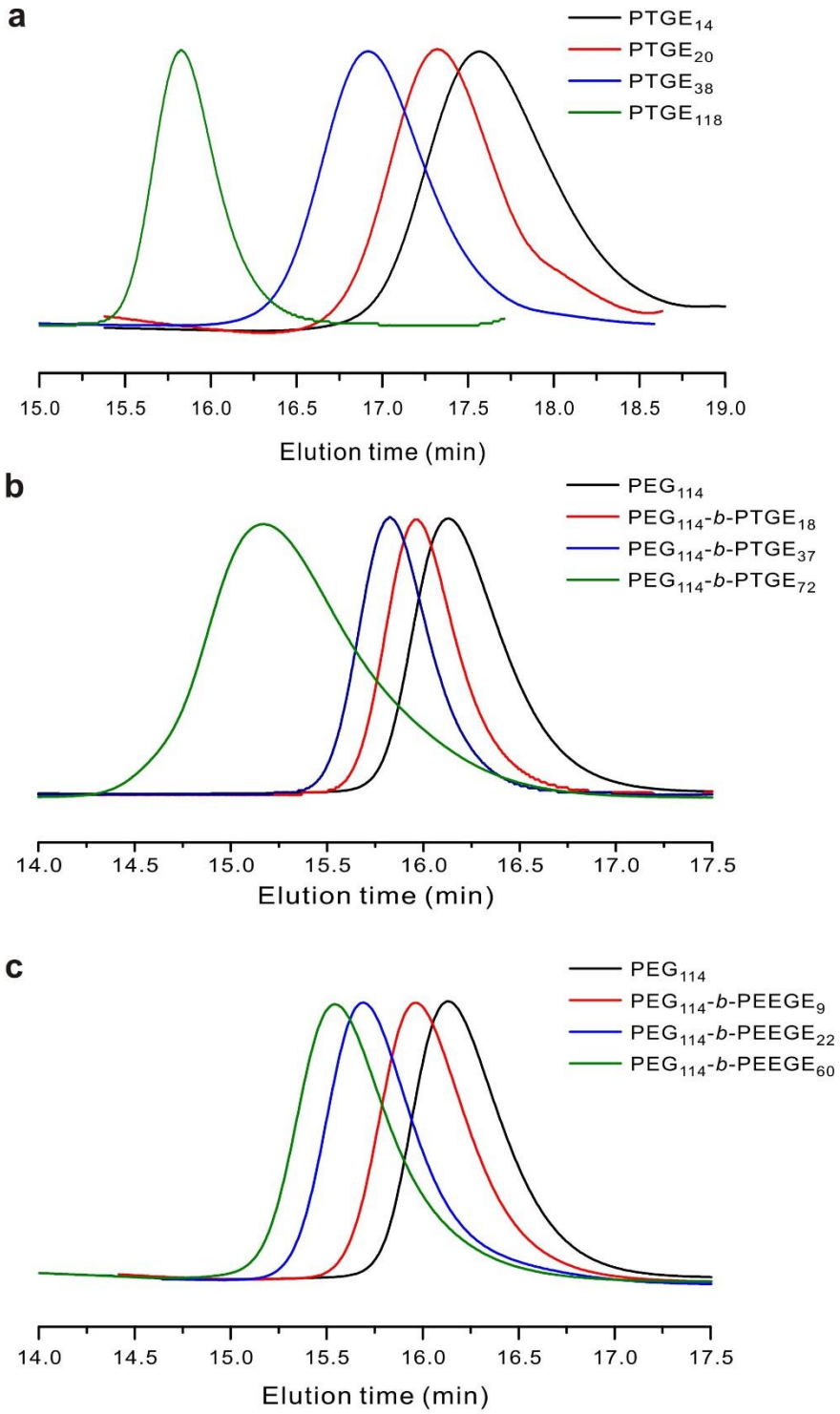

Fig. S4 GPC elution traces in THF using an RI signal and PS as a standard of (a) homopolymer $PTGE_n$, (b) block copolymer PEG_{114}-*b*-$PTGE_n$ and (c) PEG_{114}-*b*-$PEEGE_n$.

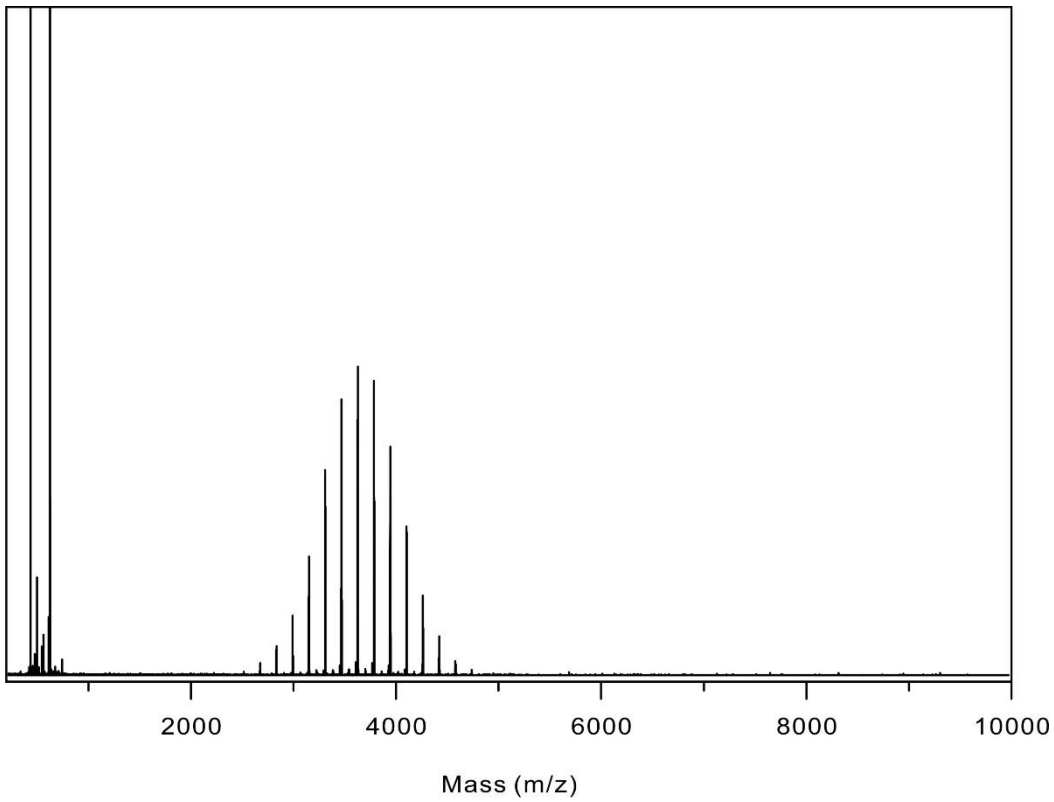

Fig. S5 Full ranges of MALDI-ToF spectrum of the $PTGE_{38}$ homopolymer. (matrix: α-cyano-4-hydroxycinnamic acid)

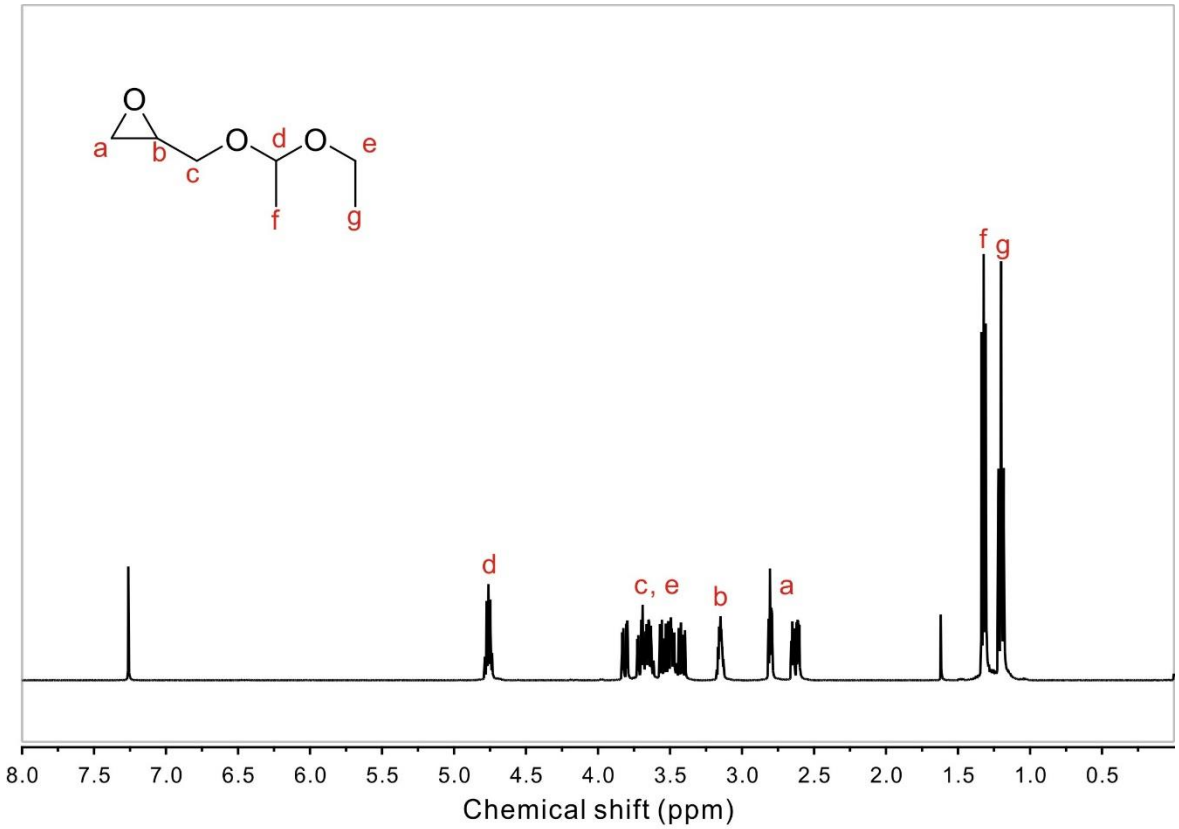

Fig. S6 400 MHz ^{1}H NMR spectrum of EEGE in $CDCl_3$.

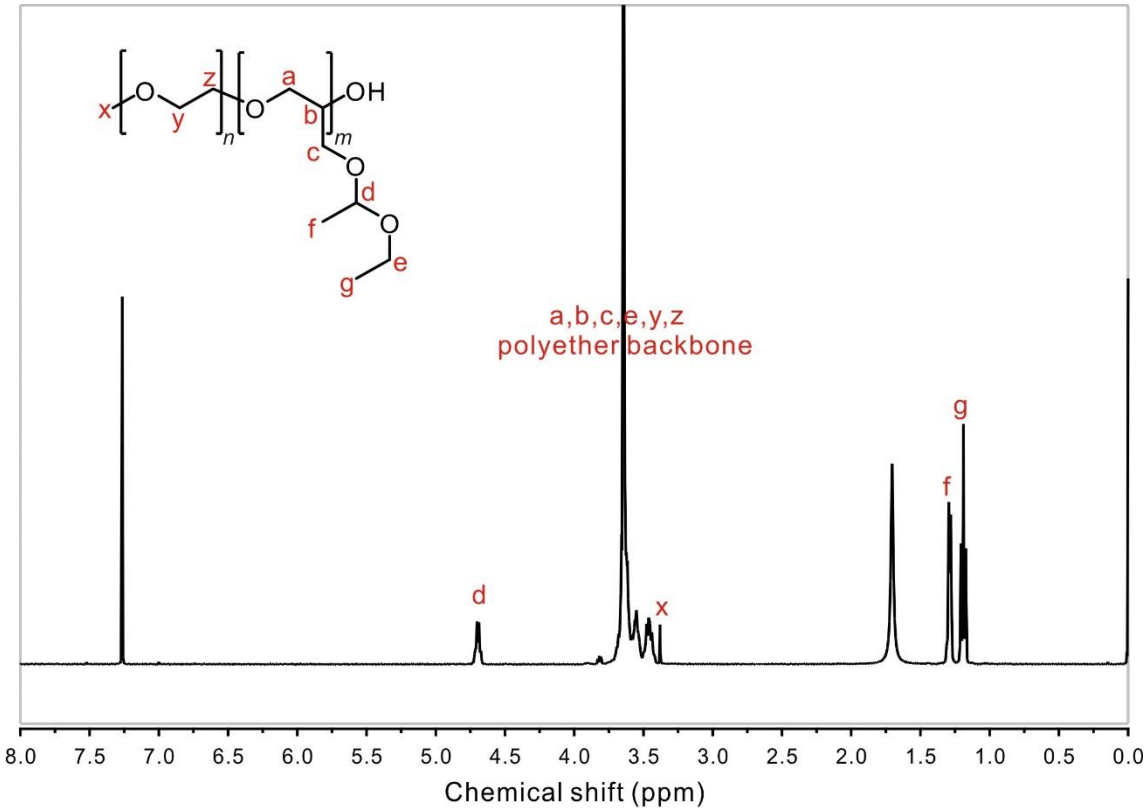

Fig. S7 400 MHz ^{1}H NMR spectrum of PEG-*b*-PEEGE in $CDCl_3$.

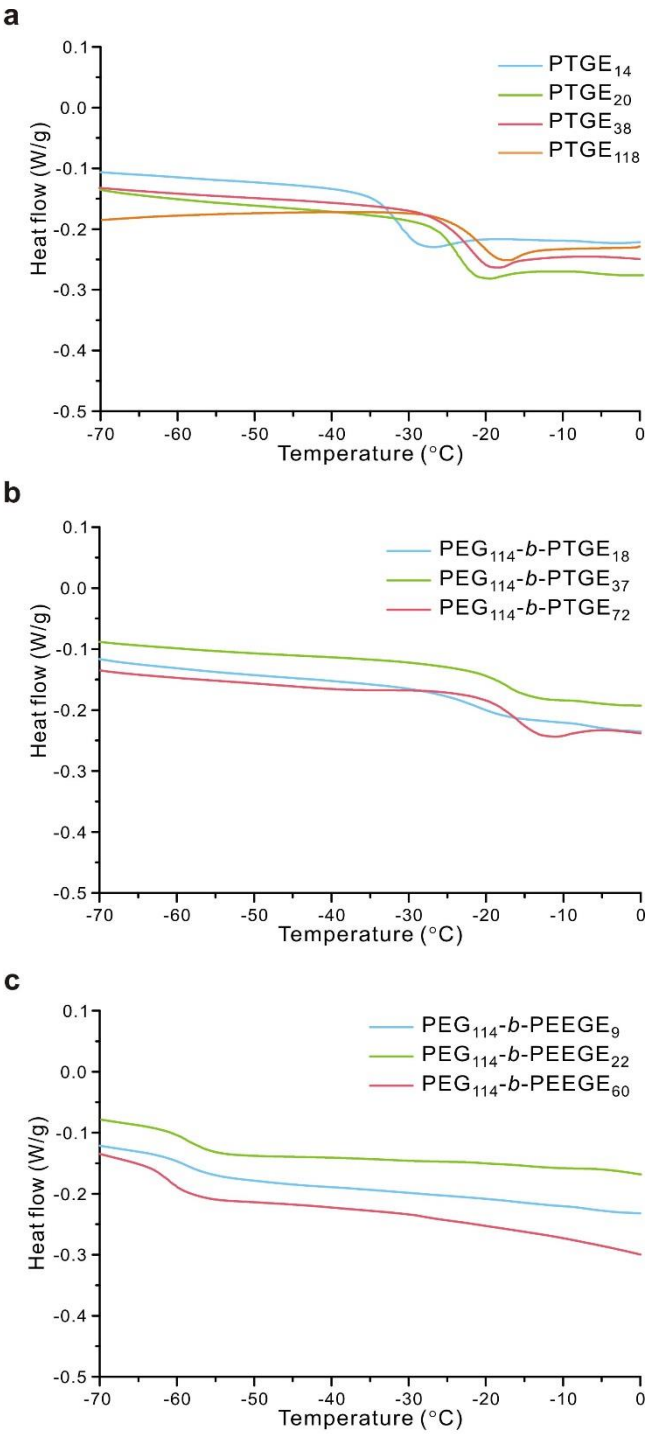

Fig. S8 DSC thermograms for (a) homopolymer PTGE$_n$ (n = 14, 20, 38, and 118), (b) block copolymer PEG$_{114}$-*b*-PTGE$_n$ (n =18, 37, and 72), and (c) block copolymer PEG$_{114}$-*b*-PEEGE$_n$ (n = 9, 22, and 60). The melting temperature of PEG block was observed at 50 − 54 °C.

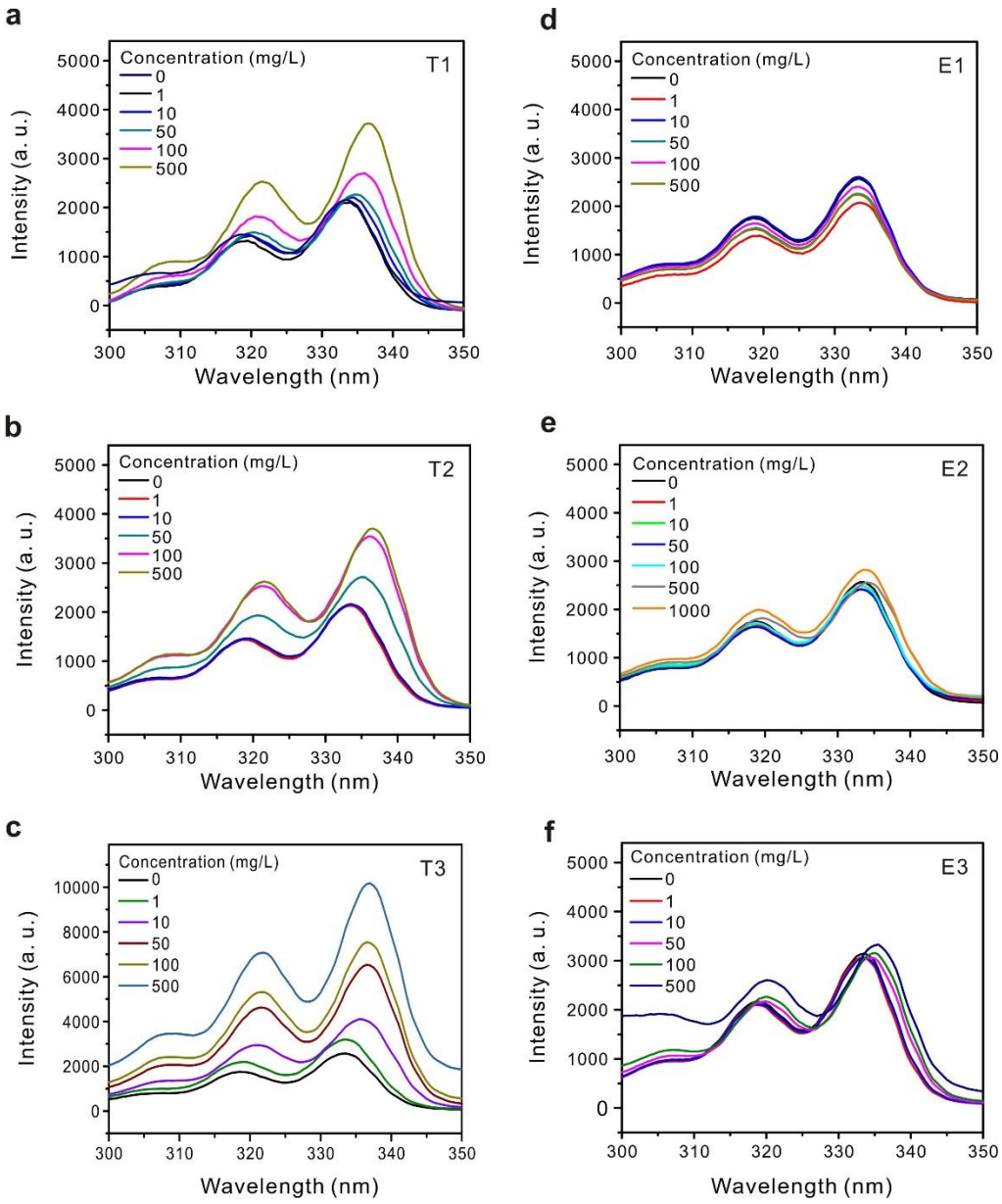

Fig. S9 Excitation spectra of pyrene in aqueous solutions of (a) **T1**, (b) **T2**, (c) **T3**, (d) **E1**, (e) **E2**, and (f) **E3** micelles at concentrations ranging from 0 to 500 mg/L (emission wavelength of 372 nm)

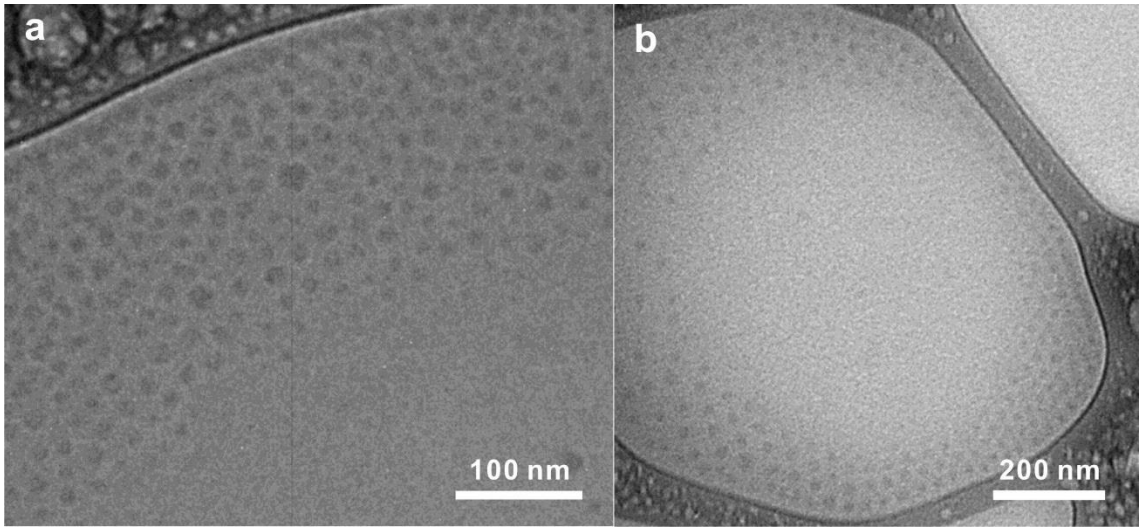

Fig. S10 Cryo-TEM images of (a) **E2** and (b) **E3** micelles.

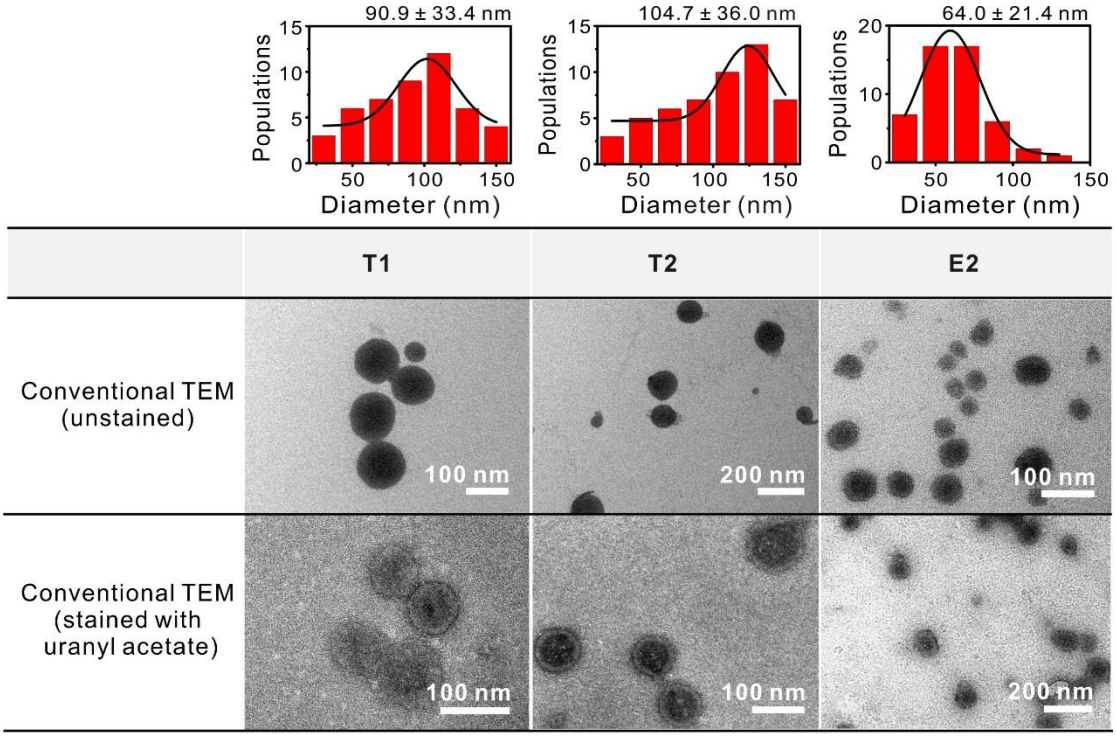

Fig. S11 Conventional TEM images of **T1**, **T2** and **E2** micelles with and without staining. Conventional TEM can induce some artifacts or large aggregates of micelles during solvent evaporation. To prevent this structural transformation by solvent evaporation, cryo-TEM was performed.

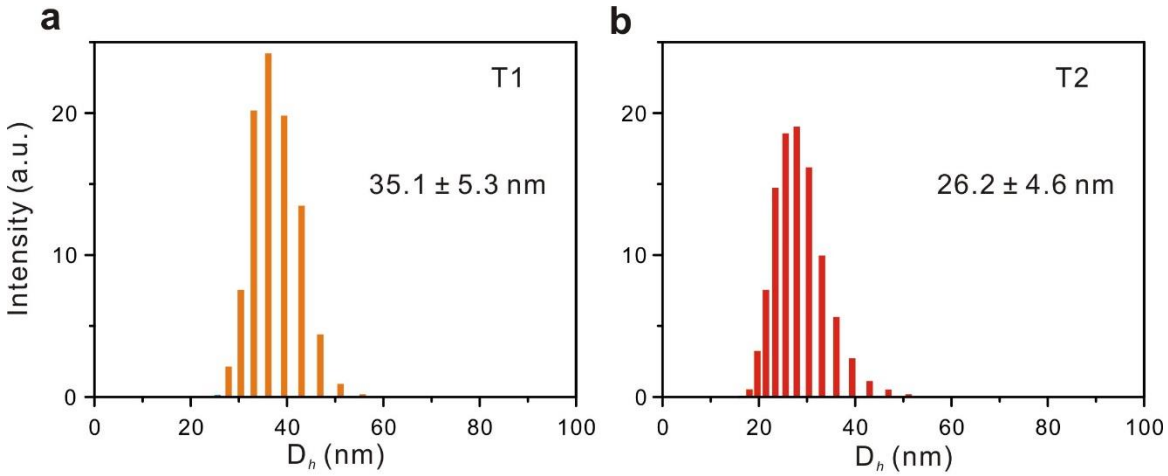

Fig. S12 Size distribution of (a) **T1** and (b) **T2** micelles determined by DLS.

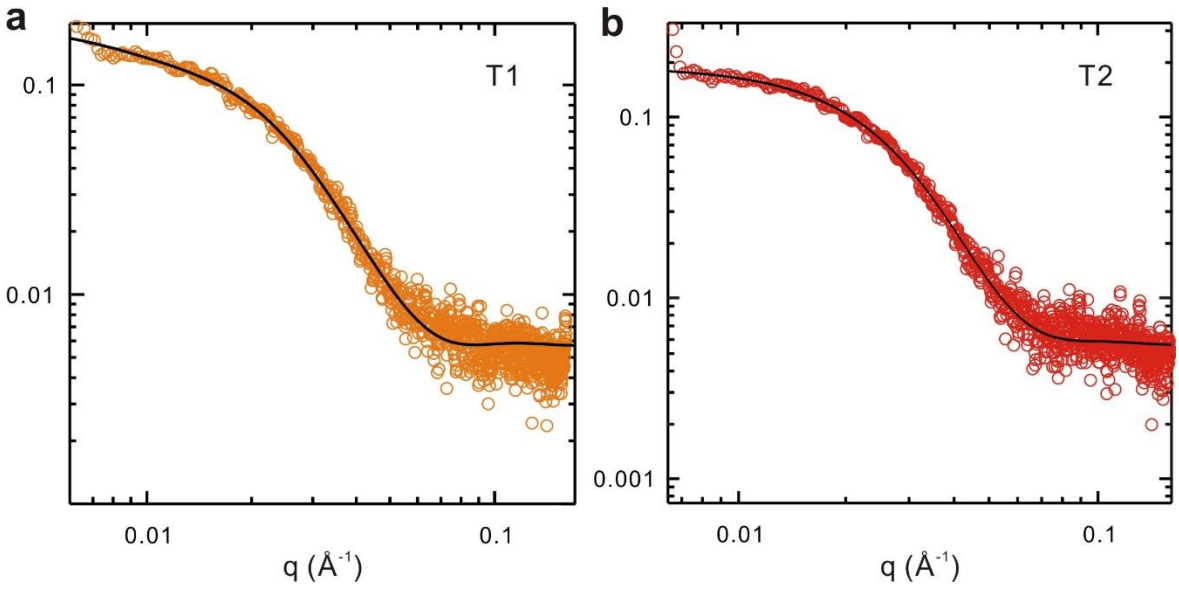

Fig. S13 Size distribution of (a) **T1** and (b) **T2** micelles determined by SAXS curves.

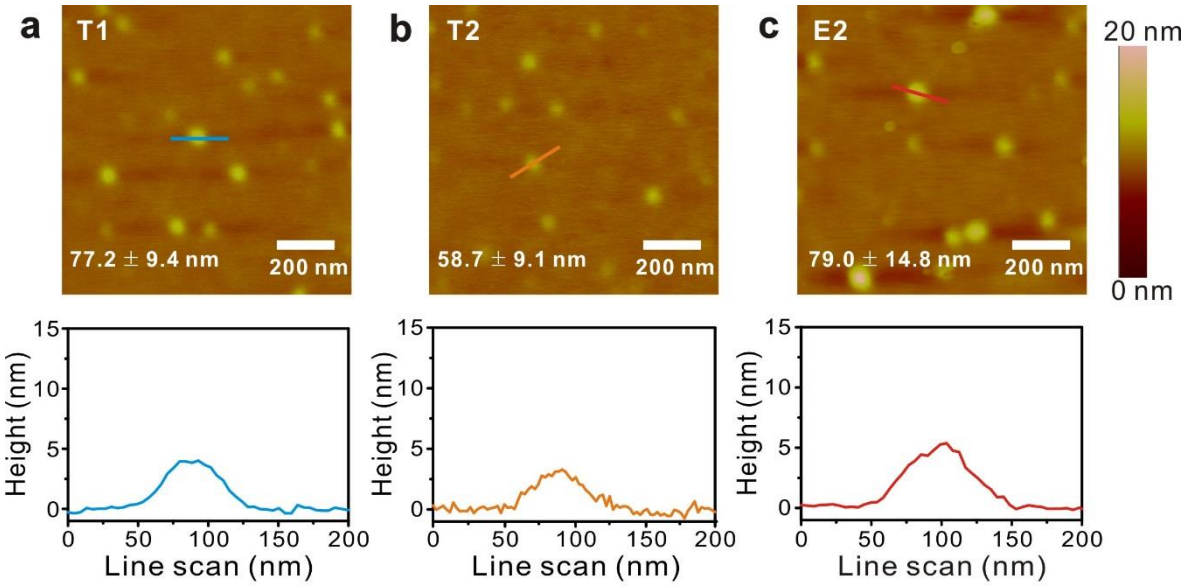

Fig. S14 AFM images and heights of (a) **T1**, (b) **T2**, and (c) **E2** micelles with an average diameter of 77.2, 58.7 and 79.0 nm, respectively.

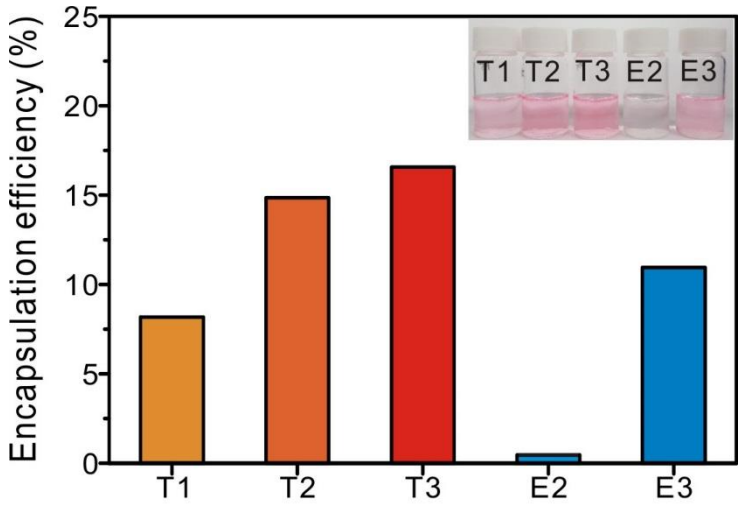

Fig. S15 Encapsulation efficiency of Nile Red in all micelles. Inset shows the suspensions of micelles containing Nile Red with varying degrees of encapsulation efficiency.

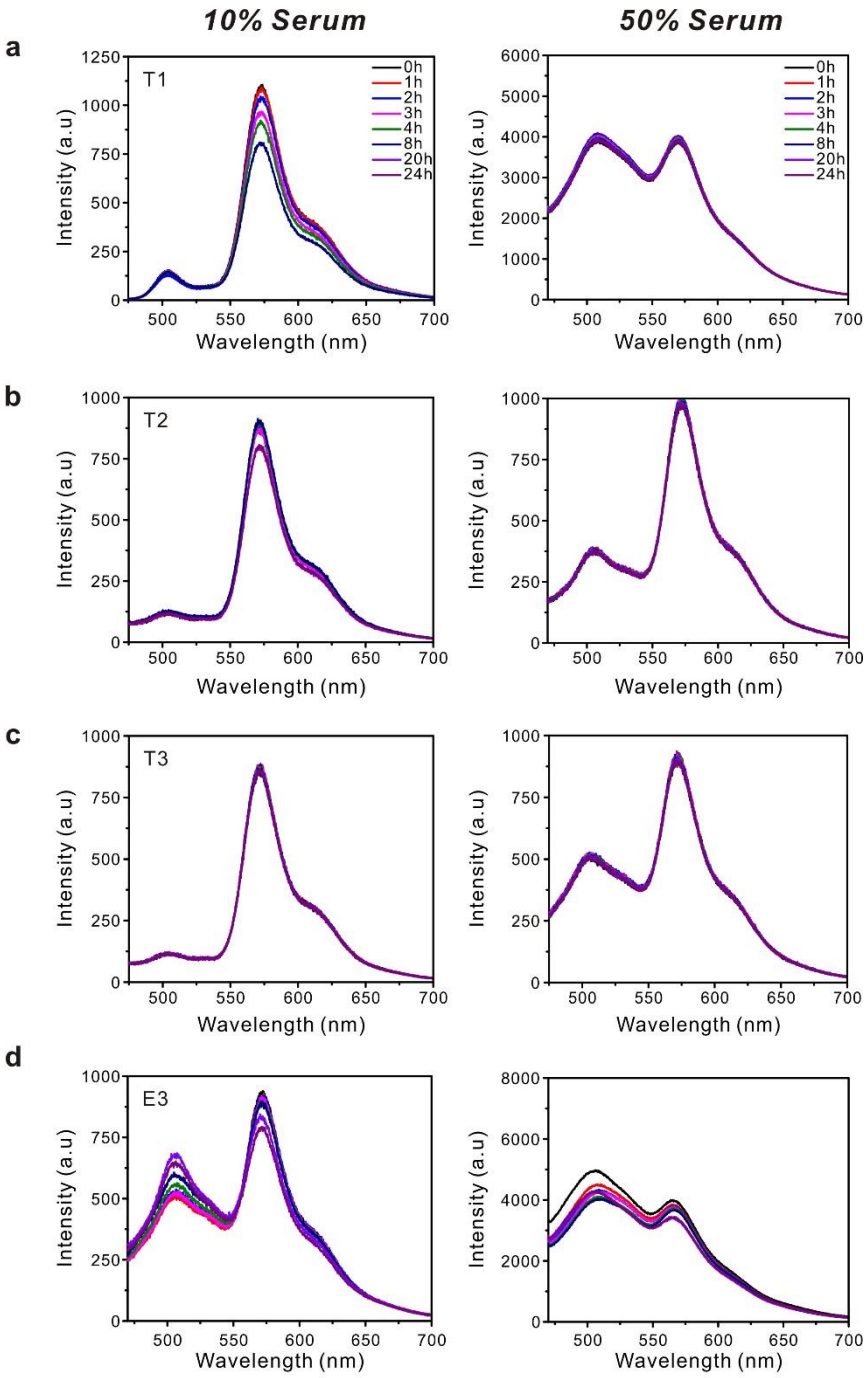

Fig. S16 FRET based encapsulation stability analysis of (a) **T1**, (b) **T2**, (c) **T3** and (d) **E3** in 10% and 50% serum. Emission peak of DiO (FRET donor) observed at 510 nm and DiI (FRET acceptor) at 570 nm.

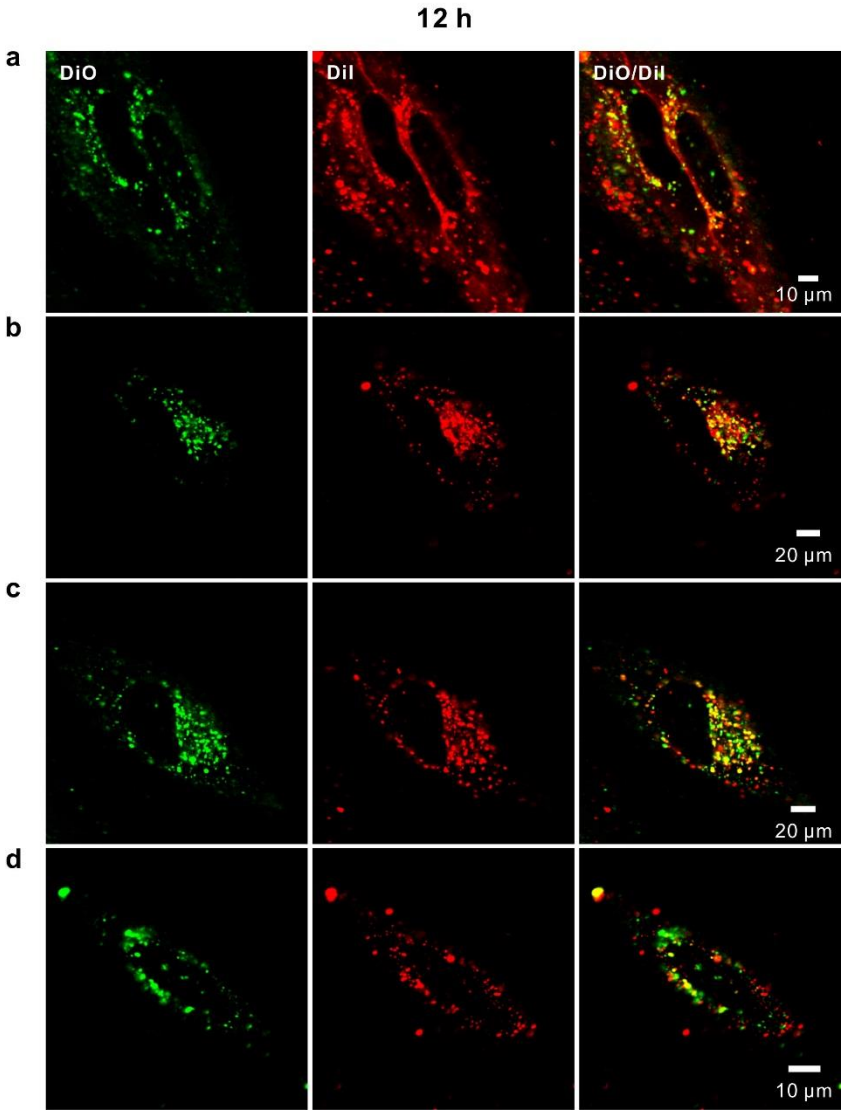

Fig. S17 *In vitro* FRET disappearance studies for (a) **T1**, (b) **T2**, (c) **T3** and (d) **E3** after 12 h incubation by live imaging in HeLa cancer cells containing 10% FBS. Excitation and emission wavelengths for DiO were 488 nm and 535 nm, respectively. Excitation and emission wavelengths for DiI were 543 nm and 620 nm, respectively.

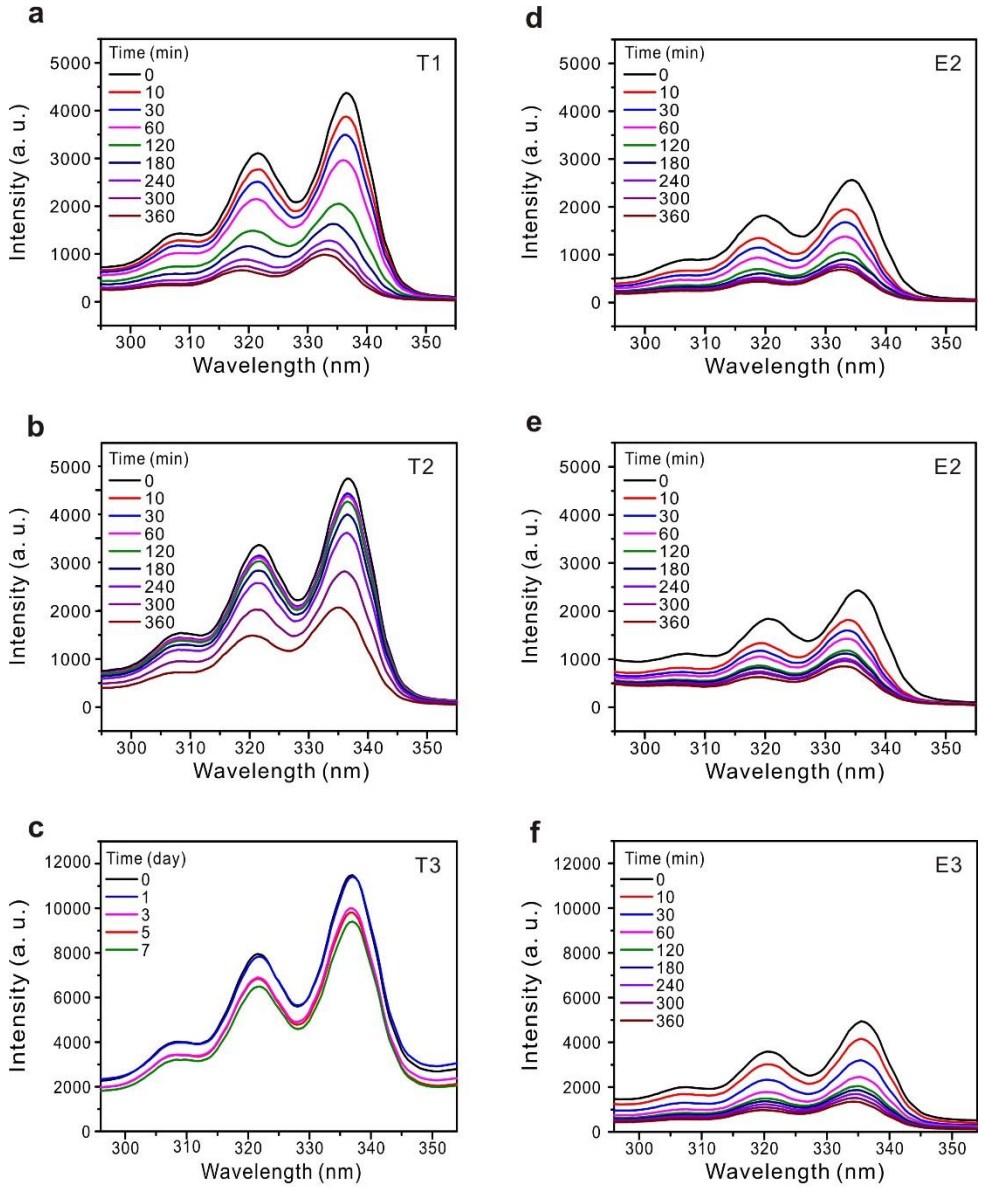

Fig. S18 Changes in excitation spectra of pyrene encapsulated by (a) **T1**, (b) **T2**, (c) **T3**, (d) **E2**, (e) **E2** and (f) **E3** micelles after acid treatment. All samples contain 1.0 mg/mL of polymer except the sample in (e) which has a concentration of 5.0 mg/mL.

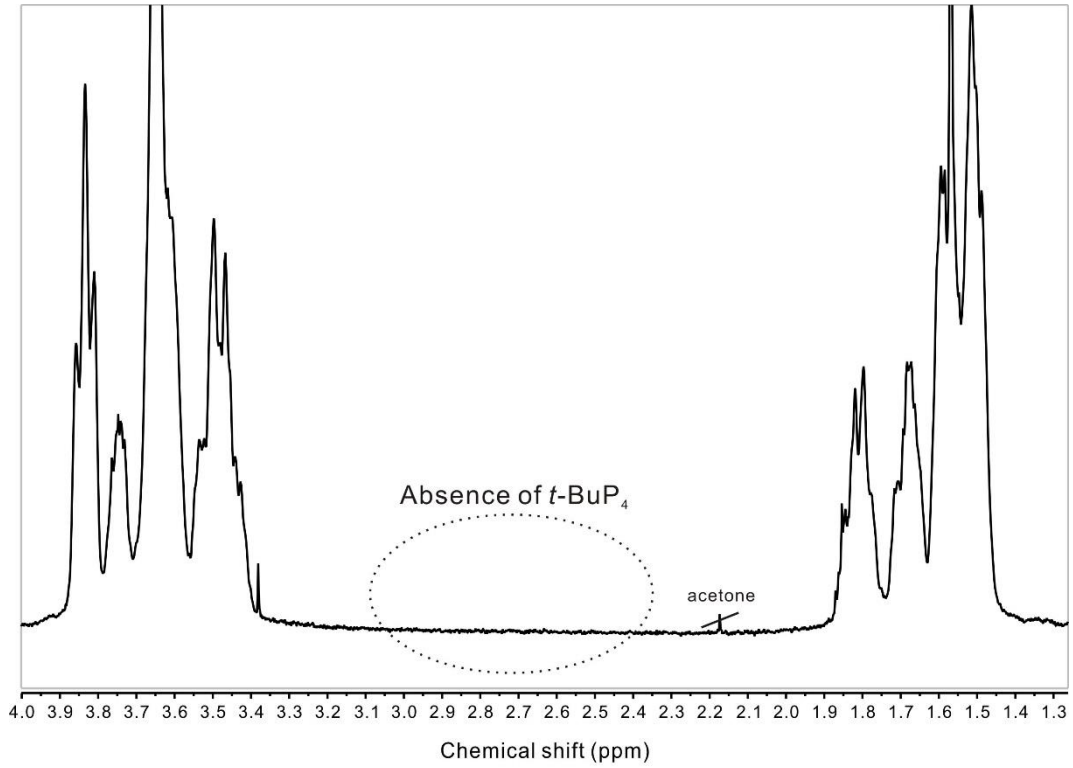

Fig. S19 Expanded ^{1}H NMR spectra of PEG_{114}-*b*-$PTGE_{37}$, displaying the clear disappearance of the residual phosphazene base, *t*-BuP_4.

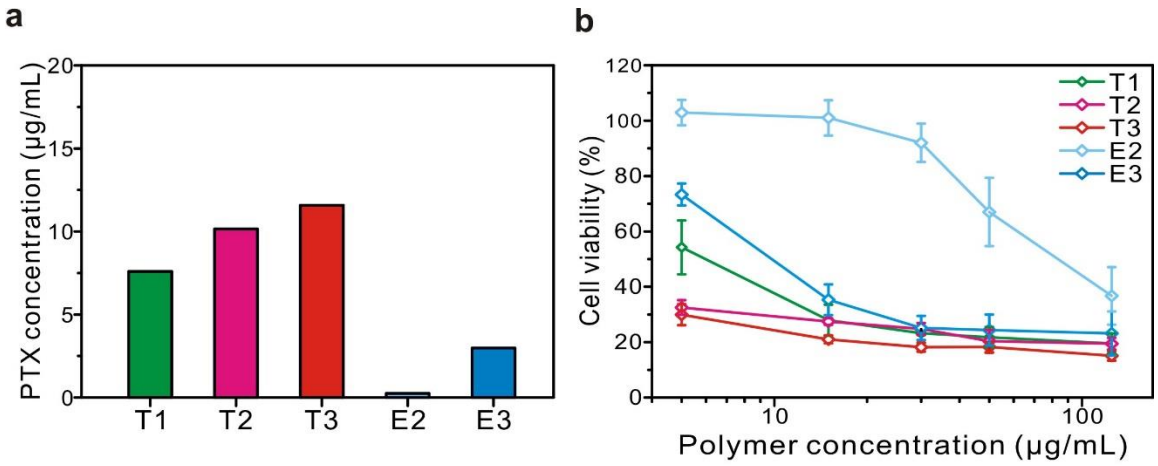

Fig. S20 (a) PTX encapsulation efficiency of **T1**, **T2**, **T3**, **E2** and **E3** micelles at 5 mg/mL polymer concentration and (b) *in vitro* cell viability of PTX-loaded micelles.